Hydrodynamic description of spectra at high transverse mass in ultrarelativistic heavy ion collisions

T. Peitzmann

Universiteit Utrecht, 3508 TA Utrecht, The Netherlands

Abstract. Transverse mass spectra of pions and protons measured in central collisions of heavy ions at the SPS and at RHIC are compared to a hydrodynamic parameterization. While the chemical temperature needed at RHIC is significantly higher compared to SPS, the spectra may be described using kinetic freeze-out parameters which are similar for both beam energies. At RHIC either the temperature or the flow velocity is higher, but the data provide no unambiguous proof for much stronger transverse flow. The contribution of such hydrodynamic emission at high transverse momenta is investigated in detail. It is shown that hydrodynamics may be relevant up to relatively high transverse momenta. The importance of the velocity profile used in this context is highlighted.

1 Introduction

The description of transverse momentum (or transverse mass) spectra with hydrodynamic models is one of the well established tools in ultrarelativistic heavy-ion physics [1–8]. The applicability of such models is still under discussion, because they require local thermalization, which may not hold for the entire reaction volume. Furthermore, at high transverse momenta hard scattering is expected to provide an important contribution to particle production – the exact momentum region where this would apply is under debate.

Comparisons to experimental data have often been performed using parameterizations of hydrodynamic distributions, which have to use simple assumptions about the freeze-out conditions, e.g. mostly one universal freeze-out temperature is used. While such parameterizations can not replace full hydrodynamic calculations, they can provide a reasonable guideline to the general behavior of particle distributions, especially as systematic studies are more accessible in this case due to the much more modest calculational effort.

In the present paper I will assume the validity of hydrodynamic pictures, but I will not attempt to deliver a full-fledged, realistic hydrodynamic calculation. A parameterization will be used to describe momentum spectra at low and intermediate m_T[1]. Parameters for chemical and kinetic freeze-out will be determined from a simultaneous fit of pion and (anti-)proton spectra. The main intention is to use a not too unrealistic hydrodynamic parameterization fitted to low transverse masses to study the extrapolation to high m_T.

---

[1] While such calculations can also be used to compare to two-particle-correlations, this will not be the scope of this paper

This is very important also in the light of recent attempts to measure jet quenching at RHIC via transverse momentum distributions [9]. If the particle emission at low m_T is governed by hydrodynamics, as e.g. the results on elliptic flow [10,11] suggest, then such a hydrodynamic source will inevitably contribute at high m_T also. Such a hydrodynamic contribution would have to be taken into account before comparing them to pQCD calculations and obtaining estimates of the amount of suppression of hard scattering.

2 The model

The calculations presented in this paper are based on a parameterization of the source at freeze-out by Wiedemann and Heinz [4] which is motivated by a hydrodynamic approach and includes effects of transverse flow and resonance decays. The original computer program calculates the direct production of pions and the contributions from the most important resonances having two- or three-body decays including pions (ρ, K_S^0, $K^\star$, Δ, $\Sigma + \Lambda$, η, ω, η'). The transverse momentum spectra of the directly emitted resonances r are given by:

$$\frac{dN_r^{\mathrm{dir}}}{dM_T^2} = \mathrm{const.} \cdot (2J_r + 1)$$

$$\times M_T \int_0^4 d\xi e^{-\xi^2/2} K_1 \left(\frac{M_T}{T} \cosh \eta_t(\xi) \right)$$

$$\times I_0 \left(\frac{P_T}{T} \sinh \eta_t(\xi) \right) , \qquad (1)$$

where $\xi = r/R$ and R is the Gaussian radius of the source. Because the integrals are evaluated numerically, fixed integration boundaries have to be chosen. The upper limit

of $\xi = 4$ was chosen to ensure that for most reasonable shapes only negligible tails of the distribution extend beyond the limits. The transverse rapidity of the source element is given as $\eta_t(\xi) = \eta_f \xi^n$, where the default value of the power is $n = 1$. The transverse rapidity parameter η_f controls the amount of transverse flow.

This distribution represents the rapidity integrated spectrum, which will be used in this paper, as it is easier to calculate compared to the general rapidity differential spectrum. In comparison to experimentally measured spectra, which are mostly from limited rapidity regions, this may introduce a bias. This bias should however be small, if the rapidity dependence of the spectra is negligible as in a longitudinal scaling expansion (Bjorken) scenario. In fact, although the Bjorken picture is not at all applicable at SPS, the dependence of the spectral shape on rapidity is already reasonably small [12]. The dependence of yields of different species on rapidity may have a small effect on the chemical parameters in the fits. We will comment on this again in a later section.

The original version of this model uses the following assumptions:

1. The spatial density distribution at freeze-out is chosen as a Gaussian.
2. One universal freeze-out temperature is used which determines both the spectral shape and the ratio of different particle species (i.e. resonances).

In the calculations performed here the model has been modified in the following way:

1. As the spatial distribution a Woods-Saxon shape:

$$\rho_{\mathrm{ws}}(\xi) = \rho_0 \cdot \frac{1}{1 + \exp \Delta(\xi - 1)} \qquad (2)$$

has been introduced. By varying the parameter Δ the shape can be adjusted. For large values of Δ the shape approaches a box-like distribution. The shape may also be chosen very similar to a Gaussian for comparison. The spatial distributions fix implicitly the shape of the velocity distribution. While this may not be very relevant at low transverse momenta, it has been shown to be important at high p_T [7]. The influence of different distributions has also been investigated in [8].
2. The spectra for a given particle (or resonance) are calculated using the kinetic temperature T_{kin}. Finally the normalization is readjusted to the chemical temperature T_{chem} assuming that dN/dy at midrapidity scales with the temperature as [1]:

$$\frac{dn_{\mathrm{th}}}{dy} = \frac{V}{(2\pi)^2} T^3 \left(\frac{m^2}{T^2} + \frac{2m}{T} + 2 \right) \exp\left(-\frac{m}{T} \right) . \qquad (3)$$

It is commonly believed that chemical freeze-out (determining particle ratios) should occur at higher temperature than kinetic freeze-out (determining the spectral shape), so at least two independent temperatures may be needed.
3. Furthermore the program has been enhanced to simultaneously describe protons and antiprotons in addition
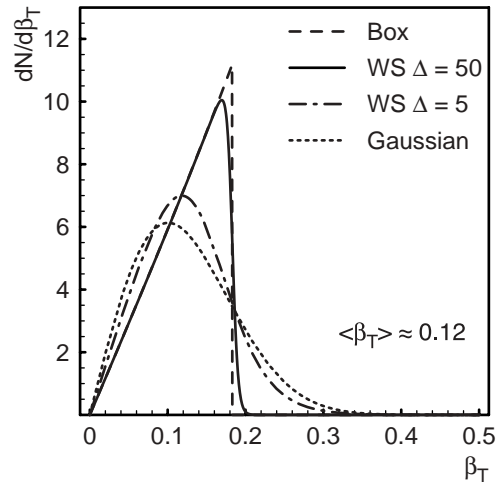
Fig. 1. Velocity distributions of the model source for different source shapes at an average velocity of $\langle \beta_T \rangle \approx 0.12$

to pions. Here the decay contributions from Δ and $\Sigma + \Lambda$ have been taken into account. This of course requires the introduction of another parameter: the baryonic chemical potential μ_B.

To better understand the importance of the different shapes of the source distribution, it is helpful to investigate the resulting velocity distributions:
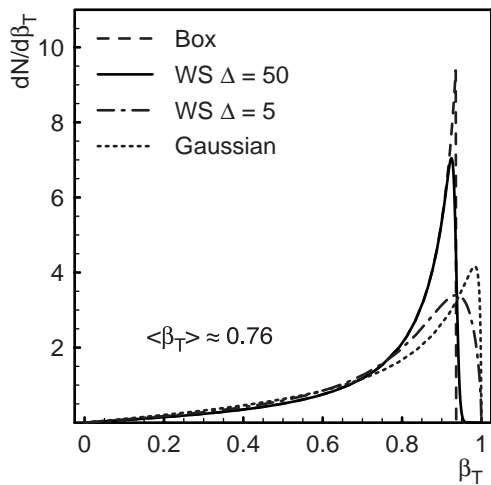
$$\frac{dN}{d\beta_T} = \frac{2\pi\xi}{\eta_f} \cdot \frac{1}{1 - [\beta_T(\xi)]^2} \cdot \rho(\xi), \qquad (4)$$

and their mean values:

$$\langle \beta_T \rangle = \frac{\int_0^4 d\xi \beta_T(\xi)\rho(\xi)}{\int_0^4 d\xi \rho(\xi)}, \qquad (5)$$

as they directly influence the shape of the momentum distribution, while the spatial distribution is actually not directly relevant. Figure 1 shows velocity distributions for different shapes at a small average velocity of $\langle \beta_T \rangle \approx 0.12$. For such small velocities the relation between rapidity and velocity $\beta_T = \tanh \eta_t$ may be approximated by a linear relation, so most of the expected properties of the distributions are preserved. One can see that the box profile yields a sharp cutoff of the velocity distribution. The Woods-Saxon with $\Delta = 50$ looks very similar to the box with a slightly smeared out edge. The Gaussian has a much more smooth edge resulting from the tail of the spatial distribution. The Woods-Saxon with $\Delta = 5$ provides a similar case as the Gaussian, both have considerable contributions at velocities much higher than the average which will finally lead to an inhanced yield at higher transverse momenta for the same inverse slope a low p_T, i.e. to stronger curvature of the spectrum.

Figure 2 shows similar distributions for a high average velocity of $\langle \beta_T \rangle \approx 0.76$. Again the box profile leads to a sharp upper limit in velocity, but the triangular shape of the distribution is distorted by the non-linearity of the relation between β_T and η_t. The Woods-Saxon for $\Delta =$

Fig. 2. Velocity distributions as in Fig. 1 at an average velocity of $\langle \beta_T \rangle \approx 0.76$
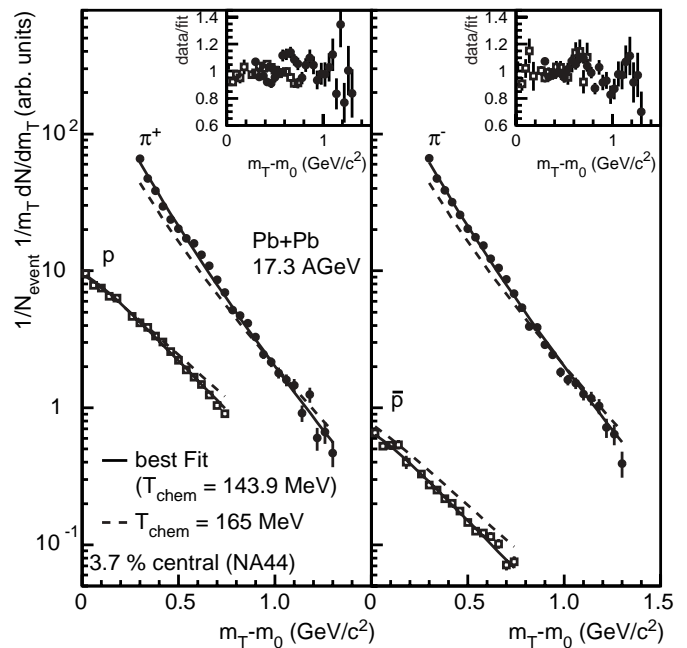

Fig. 3. Transverse mass distributions of pions and (anti-) protons for central Pb+Pb collisions at 158 AGeV from the NA44 experiment [13]. Included are two different fits to the data with the hydrodynamic model discussed in the text

50 is again similar to the box, and the one for $\Delta = 5$ and the Gaussian are also close. However, in this case the two latter distributions have a maximum shifted towards higher velocity which is also due to the non-linearity. Still, the general property of these distributions is that they have larger contributions at high velocities for the same average velocity as the other two distributions. For such large velocities it is noteworthy that the average velocity depends significantly on the recipe used to calculate it. If instead of (5) one uses:

$$\langle \beta_T \rangle' = \frac{\int_0^4 d\xi \beta_T(\xi) \gamma_T(\xi) \rho(\xi)}{\int_0^4 d\xi \gamma_T(\xi) \rho(\xi)}, \qquad (6)$$

the numerical values are larger by almost 10%, and differ slightly for the different profiles. I will use the definition (5) throughout.

3 Hadron spectra from SPS

The model described above has first been compared to data from SPS heavy ion experiments. Data on pion, proton and antiproton production in the 3.7 % most central Pb+Pb collisions from NA44 [13] and in the 10 % most central Pb+Pb collisions from NA49 [14,15] have been used. The transverse mass spectra of NA44 are shown in Fig. 3, they cover the range of $0.3\,\mathrm{GeV}/c^2 \leq m_T - m_0 \leq 1.3\,\mathrm{GeV}/c^2$ for pions and $0.02\,\mathrm{GeV}/c^2 \leq m_T - m_0 \leq 0.74\,\mathrm{GeV}/c^2$ for protons and antiprotons. The model has been fitted to the data. The best agreement can be achieved with a kinetic temperature $T_{kin} = 122.2$ MeV, an average transverse flow velocity $\langle \beta_T \rangle = 0.478$, a chemical temperature $T_{chem} = 143.9$ MeV and a baryonic chemical potential $\mu_B = 193.3$ MeV. For this fit the width parameter has been set to $\Delta \equiv 50$, allowing for a free variation of this parameter produces a slightly smaller value with a very large error while the other parameters remain unchanged. As the fits seem to be insensitive to small changes
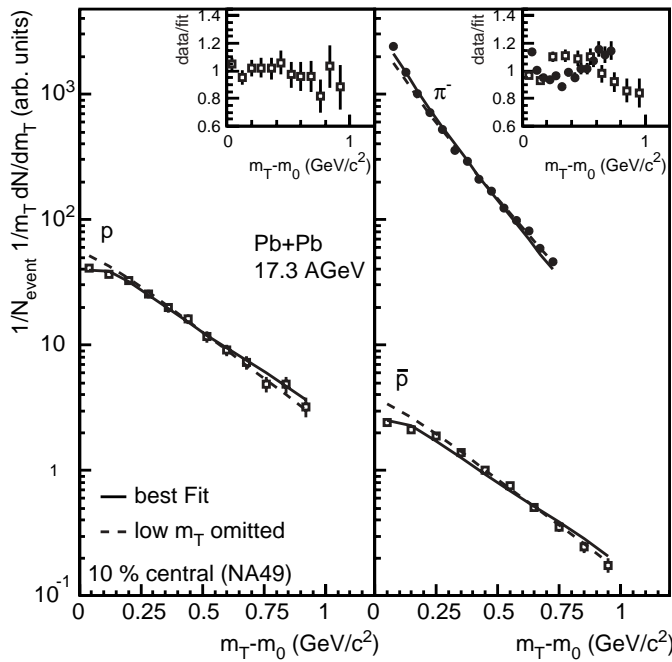
in Δ, we have performed most fits with a fixed value. For systematic checks some of the constraints on the fits have been varied. Most of these changes, as e.g. omitting some of the data points (the lowest or highest in m_T, resp.) from the fit, do not affect the parameter values significantly. Significant changes are obtained under the following conditions:

1. All contributions from weakly decaying particles are ignored.
   In this case the chemical temperature and the baryonic chemical potential change slightly, while the kinetic temperature and the flow velocity are essentially unaltered. This is understandable as the particle ratios may depend more strongly on this contribution than the shape of the spectra. As the quality of the fit is similar to the best fit above and a not precisely specified fraction of weak decays may contribute to the data, this has to be taken into account in the systematic error.
2. The width parameter is set to $\Delta \equiv 5$.
   In this case the chemical parameters show small changes, while the temperature and flow velocity change more significantly. This is mainly due to the fact that this spatial distribution, which is similar to a Gaussian, results in a broader velocity distribution. The quality of the fit is significantly worse than the fits given above.
3. The kinetic and chemical temperatures have been set to the same value of $T \equiv 144$ MeV and the chemical potential to $\mu_B = 193.3$ MeV.

Table 1. Fit parameters of hydrodynamic fits to pion and (anti-)proton spectra in central Pb+Pb collisions at the CERN SPS. The errors given are statistical. No error indicates that this parameter was fixed in the fit

Remarks	χ^2/ν	T_{kin} (MeV)	η_f	$\langle\beta_T\rangle$	T_{chem} (MeV)	μ_B (MeV)	Δ
			NA44 data				
best fit	217/82	122.2 ± 1.9	0.805 ± 0.007	0.478 ± 0.004	143.9 ± 0.6	193.3 ± 0.9	50
no weak decays	217/82	120.4 ± 1.9	0.804 ± 0.007	0.478 ± 0.004	150.9 ± 0.4	202.6 ± 0.9	50
broad profile	360/82	95.6 ± 3.0	0.745 ± 0.010	0.517 ± 0.007	146.3 ± 0.4	196.4 ± 0.9	5
$T_{kin} = T_{chem}$	358/85	144	0.728 ± 0.004	0.442 ± 0.002	144	193.3	50
high $\langle\beta_T\rangle$	799/83	92.7 ± 0.9	0.968 ± 0	0.55	144.6 ± 0.4	193.2 ± 0.9	50
high T_{chem}	2394/83	156.3 ± 3.0	0.802 ± 0.001	0.477 ± 0.001	165	208.4 ± 0.8	50
			NA49 data				
best fit	129/31	75.8 ± 1.9	0.968 ± 0.010	0.550 ± 0.004	133.2 ± 0.5	184.5 ± 2.0	50
low m_T omitted	16/22	108.0 ± 6.6	0.828 ± 0.034	0.489 ± 0.016	136.6 ± 0.9	184.6 ± 3.3	50

Fig. 4. Transverse mass distributions of pions and (anti-)protons for central Pb+Pb collisions at 158 AGeV from the NA49 experiment [14,15]. Included are two different fits to the data with the hydrodynamic model discussed in the text

be the different integration region in rapidity compared to [16]. If e.g. the rapidity distribution of protons is broader than the one of pions this may easily explain the smaller chemical temperature obtained here. However, for the purpose of this paper, we will just note this discrepancy and use the fit results as they are. The parameters obtained apparently describe the particle ratios at midrapidity investigated here, and this may be the relevant information which should be used also in estimating the contribution of resonances to the momentum spectra at this given rapidity.

Furthermore, it may be that part of the longitudinal motion of the source is not generated hydrodynamically but is a remnant of the initial state motion, which may be even more likely for participant protons. In this case it is not completely obvious, whether the protons observed at very different rapidities share the same chemical freeze-out temperature. If the spacetime-momentum correlation originates from a very early phase of the collision, a unique chemical temperature might not be applicable and the use of integrated multiplicities might be misleading. Rather, there is the possibility of a local temperature which may be applicable for limited rapidity regions.

The fit parameters obtained from the fits discussed above are summarized in Table 1. None of the fits provides a perfect agreement with the data, which is due to a structure in the experimental spectra which can not be described within this model.

The transverse mass spectra of NA49 cover the range of $0.05 \,\mathrm{GeV}/c^2 \leq m_T - m_0 \leq 0.75 \,\mathrm{GeV}/c^2$ for pions and $0 \,\mathrm{GeV}/c^2 \leq m_T - m_0 \leq 1 \,\mathrm{GeV}/c^2$ for protons and anti-protons, they are shown in Fig. 4 together with fits of the model. As pions and protons are not available for the same centrality selection – pions have been measured for 5 % central and (anti-)protons for 10 % central – the pions have been rescaled by a factor of 1/1.08 according to the number of participants in both samples [17]. This will introduce an additional systematic error to the chemical parameters of the fits, which depend most significantly on

Here, the flow velocity obtained is smaller than in the best fit, as is expected for a higher kinetic temperature. Again the fit quality is worse.

4. The expansion velocity has been fixed to a value of $\langle\beta_T\rangle = 0.55$. The fit quality is much worse than the best fit.

5. The chemical temperature has been set to $T_{chem} \equiv 165\,\mathrm{MeV}$ similar to results from fits of hadrochemical models to ratios of total multiplicities of different species [16].
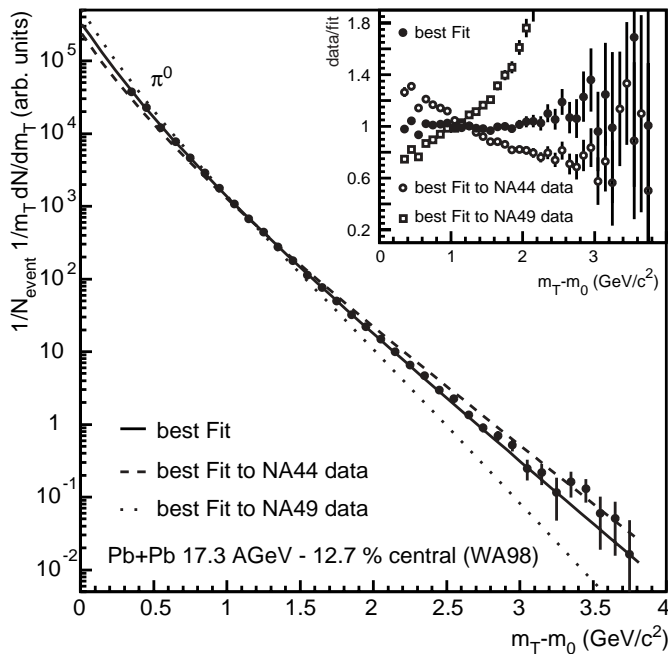
   This fit cannot describe the spectra, it essentially has the wrong ratio of pions to protons. Of importance may

Fig. 5. Transverse mass distributions of neutral pions for the 12.7% most central Pb+Pb collisions at 158 AGeV from the WA98 experiment [18]. Included are two different fits to the data with the hydrodynamic model discussed in the text

the relative normalization of different species. The fitting conditions have been varied as above, the relative variation of the parameters is also similarly small. In fact, the chemical parameters are relatively similar with slightly smaller values compared to the NA44 data. However, for these data the best agreement can be achieved with a very low kinetic temperature $T_{kin} = 75.8$ MeV and a very high average transverse flow velocity $\langle \beta_T \rangle = 0.55$. It turns out that this significant difference to the NA44 data is to a large extent due to the behavior of the data (particularly of the protons and antiprotons) at very low m_T. If the lowest three data points of all spectra are omitted from the fit, a kinetic temperature $T_{kin} = 108.0$ MeV and an average transverse flow velocity $\langle \beta_T \rangle = 0.489$ are obtained with a much better χ^2. The parameters of this fit are relatively close to those obtained from the fit to NA44 data. The low m_T data points of NA49 appear to disagree with the measurements by NA44. It is also seen from the best fit to NA49 data that the agreement is not perfect if all data points are included – there is a tendency of a larger inverse slope of the fit compared to the data especially for the antiprotons.

While the data used above have a limited range in transverse mass, one might also consider comparing such hydrodynamic distributions to data with a wider transverse momentum range. This has actually been done before at the SPS by WA98 [7], using also a program derived from the one of Wiedemann and Heinz [4]. However in this version the original assumption of the same temperature both for chemical and kinetic freeze-out was applied. Also, only neutral pion spectra were used, which give very limited information to determine all relevant parameters.

In the following, information from the above fits will be used while fitting the neutral pion spectra of WA98 [18]. Ideally one might just try to use exactly the same fits and compare it to the neutral pions. As the data are from different experiments and do not exactly use the same centrality selections, the normalization has to be kept as a free parameter. The centrality selections used below should however be similar enough, so that the shape of the spectra should not differ strongly.

In Fig. 5 fits using the parameters obtained above are compared to the neutral pion spectra for the 12.7% most central reactions of Pb+Pb at 158 AGeV. The "best fit" to NA44 in Table 1 is shown as a dashed line, the one to NA49 data as a dotted line. The description is only superficially adequate. The fit to NA44 overshoots the data at large transverse masses, and one obtains a $\chi^2/\nu = 712/20$. The fit to NA49 is below the data at large transverse masses with a $\chi^2/\nu = 1395/20$. This large difference for the pion spectra at high m_T is of course due to the much larger flow velocity for the NA49 fit, which increases the proton inverse slope while decreasing the one of the pions compared to NA44. Another fit has been performed keeping only the parameters T_{chem} and μ_B the same as in the earlier fit and optimizing the kinetic temperature and the flow for the neutral pions. This fit (shown as a solid line) yields a good description with $\chi^2/\nu = 27/18$. The fit parameters obtained are $T_{kin} = 130.3$ MeV and $\langle \beta_T \rangle = 0.415$. The (dis-)agreement of the fits can also be judged from the inset in Fig. 5, which shows the ratios of the data to the fits.

One might argue that the different centrality selections are responsible for the disagreement. Although this does not seem to be very likely, as it has been shown [18], that the shape of the pion spectra does not vary strongly for medium-central to central collisions, a comparison to the 1% most central data has been performed. The results are displayed in Fig. 6. Again the dashed and dotted lines show fits with all parameters fixed as above from NA44 and NA49. The behavior of the fits is qualitatively similar to the one discussed above, the disagreement of the NA49 fit to the data is not as pronounced as before, which is due to the slightly steeper spectra in this case. The solid line shows a good fit with $T_{kin} = 113.0$ MeV and $\langle \beta_T \rangle = 0.459$. The different parameters for this second fit compared to the other central (12.7%) sample are most likely not conclusive, but are an example that fitting momentum spectra of just one particle species leaves an ambiguity in the parameters. The higher flow velocity can be compensated by a lower temperature and vice versa. Also I will not put too much emphasis on the fact that the fits to the NA44 data appear to overpredict the pion yield at high p_T, because part of this discrepancy might be due to systematic differences between the two experiments involved.

As one of the major uncertainties in this analysis appears to be related to different experimental data sets, it may be worthwhile to compare data of NA44 and NA49 directly. This has been done in Fig. 7 by plotting the ratio of the data to the best fit of the parameterization to NA44 data (first row in Table 1). The same fit is used
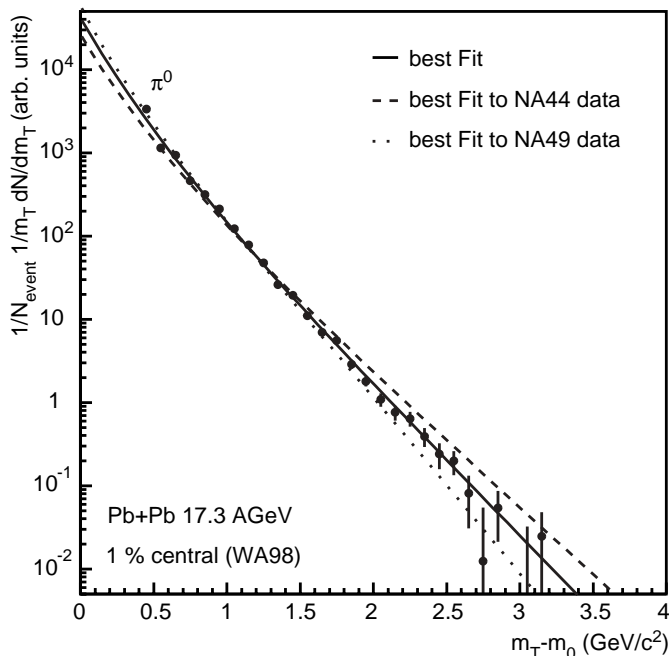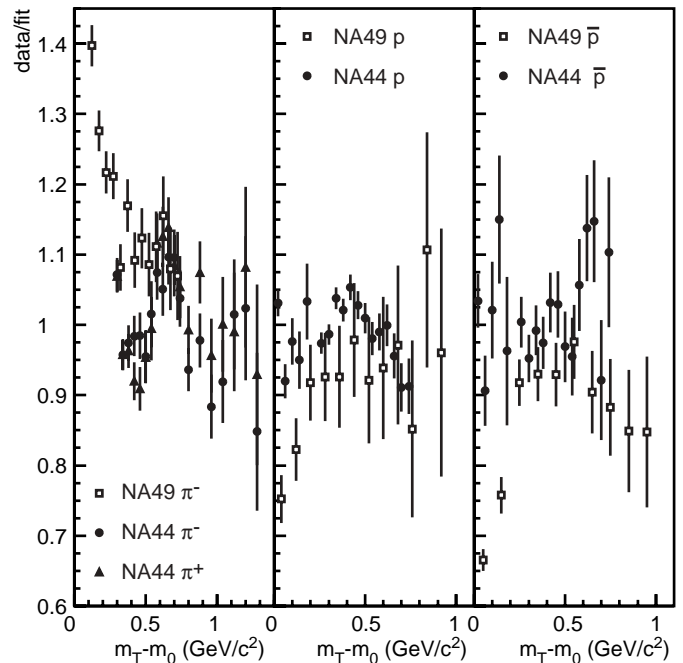
Fig. 6. Transverse mass distributions of neutral pions as in Fig. 5 for the 1% most central Pb+Pb collisions at 158 AGeV from the WA98 experiment [18]


Fig. 7. Ratios of experimental transverse mass distributions of pions (*left*), protons (*center*) and antiprotons (*right*) to a fit of the hydrodynamical parameterization for central Pb+Pb collisions at 158 AGeV from NA44 and NA49

for both data sets, there is one overall normalization for all species which differs between experiments. One can clearly see that the deviations are most significant at low m_T for protons and antiprotons. In the systematic studies it was found that the parameters for the fits to NA44 do not depend very much on the fitting range, while the parameters for NA49 change significantly when the lowest m_T data points are not used. It should also be noted that these fits use data with statistical errors only, as systematic errors were not readily available for all data sets. If systematic errors would account for a significant fraction of the discrepancy between the two experiments, a simultaneous fit might be possible and yield more conclusive information. This could not be attempted in this paper.

One can however note that the hydrodynamic parameterization can account for a large fraction of the pion production at high p_T, even if a profile with a negligible tail towards higher velocities ($\Delta = 50$ – similar to the box profile) has been used. A more diffuse profile ($\Delta = 5$) would necessarily lead to a larger yield at high p_T. Most of the other systematic variations studied do not lead to significant variations in this respect. The most important uncertainty relates to the discrepancy already seen between NA44 and NA49. Ignoring the very low m_T data points of NA49 leads to a moderately high flow velocity. In this case the pion spectra may be almost entirely be explained by such a source. A very high flow velocity as suggested by the low m_T NA49 data would considerably reduce the hydrodynamic yield of pions at high m_T.

A fixed chemical temperature of $T_{chem} \equiv 165$ MeV leads to different results, but from Fig. 3 it is obvious that this would also lead to a larger overprediction at high p_T.

As sketched above, there may be reasons why this assumption may not be adequate for our analysis. In fact, it has been remarked in [19,20] that there is a rapidity dependence of chemical parameters. The chemical temperature of $T_{chem} = 143.9$ MeV and the baryo-chemical potential of $\mu_B = 193.3$ MeV of the best fit can be compared to results of other analyses. As stated above, the temperature is lower than the values of $T_{chem} = 158 \pm 3$ MeV [21] and $T_{chem} = 168 \pm 2.4$ MeV [16] obtained from rapidity integrated yields, but compares well with the result $T_{chem} = 141 \pm 5$ MeV given in [13].

4 Hadron spectra from RHIC

The situation at RHIC is more favorable for this analysis, as there exist data on different particle species partially reaching out to large p_T measured under the same conditions within one experiment. The PHENIX experiment has presented spectra of neutral pions [9] and identified charged hadrons [22,23] in central Au+Au collisions at $\sqrt{s_{NN}} = 130$ GeV. I will also use the data from the STAR experiment [24–26], which only cover low m_T. From the STAR experiment, the most recent data on protons and antiprotons use a sample of the 6% most central collisions, while the pions have been extracted from the 5% most central collisions. I will ignore this difference, as it should not significantly affect the shapes of the spectra, however, there may be small effects on the relative normalization which would result in an additional systematic error for the chemical parameters.
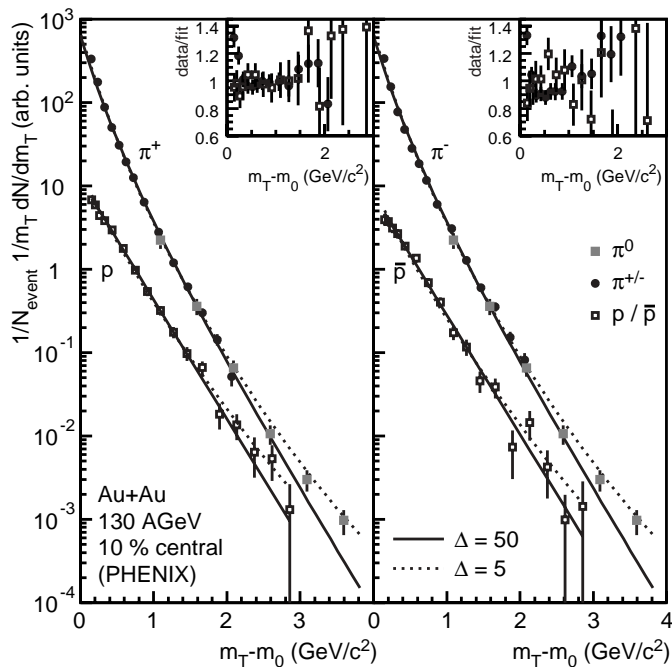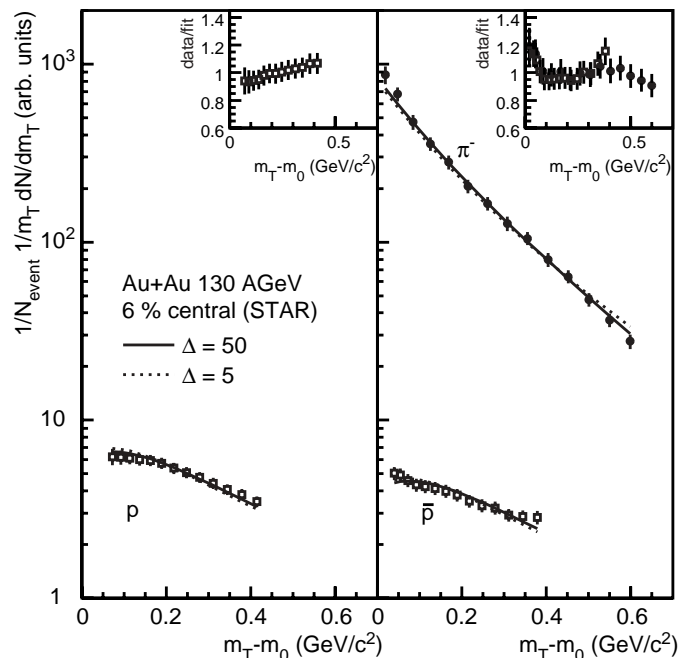
Fig. 8. Transverse mass distributions of pions and (anti-) protons for the 10% most central Au+Au collisions at $\sqrt{s_{NN}} = 130$ GeV from the PHENIX experiment [9,22,23]. The lines show fits (A) and (A′) from Table 2. The inset shows the ratio of the data to fit (A)

Fig. 9. Transverse mass distributions of protons and antiprotons for the 6% most central Au+Au collisions at $\sqrt{s_{NN}} = 130$ GeV and for negative pions for the 5% most central Au+Au collisions from the STAR experiment [24–26]. The lines show fits (B) and (B′) from Table 2. The inset shows the ratio of the data to fit (B)

A similar procedure as for the SPS data above is followed, with the addition of using p_T dependent systematic errors. For this a systematic error of 5% added in quadrature to the errors for the PHENIX data (which contain part of the systematic error already) has been assumed [27]. For STAR data a systematic error of 8% has been used for the antiproton spectra [24]. The proton and pion spectra [25,26] were already quoted with a systematic error. These does not include all of the normalization errors, so they might still further affect the chemical parameters extracted. Fits are performed to the charged pions for $m_T - m_0 < 2$ GeV/c and to (anti)protons for $m_T - m_0 < 3$ GeV/c. Systematic variations of the fitting assumptions are done as above. In addition I have studied fits to a limited transverse mass range $m_T - m_0 < 1.5$ GeV/c for pions and (anti)protons in PHENIX.

The results are summarized in Table 2, a comparison of some of the fits to the PHENIX data is shown in Fig. 8, those to the STAR data are displayed in Fig. 9.

The fits to PHENIX data show slightly better agreement for a wide profile ($\Delta = 5$), however, the difference in χ^2 is small. As can be seen in Fig. 8, the fit for $\Delta = 5$ (dotted line) has a more important contribution at high p_T. The STAR data are generally better described using the narrow profile, the differences are, however, not easily discernible in Fig. 9. For PHENIX, the two different kinds of fits yield very similar fit parameters, while there are slightly stronger variations when looking at the STAR data. As there does not seem to be a strong preference for the wider profile in any of the data sets and

as there are also theoretical arguments from true hydrodynamical calculations [28], I will base most of the discussion below on the fits with a narrow profile. For both data sets fits ignoring weak decays yield higher chemical temperatures and slightly lower kinetic temperatures. The biggest difference is again between the two experiments. The chemical parameters still show only a small effect, e.g. while fit (A) to PHENIX data yields $T_{chem} = 173.3$ MeV and $\mu_B = 35.9$ MeV, the values for STAR (B) are slightly smaller with $T_{chem} = 165.3$ MeV and $\mu_B = 31.2$ MeV. These values are similar to the results in [29] where $T_{chem} = 174 \pm 7$ MeV and $\mu_B = 46 \pm 5$ MeV are given. The better agreement at RHIC compared to SPS of the chemical parameters of this analysis with those of the integrated yields may be related to the fact that boost invariance is a much better approximation in the RHIC case. Larger differences are seen for the kinetic parameters. Fit (A) yields $T_{kin} = 143.0$ MeV and $\langle \beta_T \rangle = 0.450$, fit (B) $T_{kin} = 94.8$ MeV and $\langle \beta_T \rangle = 0.578$. As a check also fits have been performed which use the kinetic temperature from one experiment as a fixed parameter in a fit to the other experiment, and vice versa. A reasonable fit to the STAR data (with a higher χ^2) can be obtained this way by using a high kinetic temperature, but the flow velocity turns out to be larger than for PHENIX. In the other case, the fit to PHENIX data with a low temperature yields a much higher χ^2 – no good fit can be obtained. There have been fits to the PHENIX data using hydrodynamic parameterizations that do not in-

Table 2. Fit parameters of hydrodynamic fits to pion and (anti-)proton spectra in central Au+Au collisions at RHIC. The errors given are fit errors using statistical and partial systematic errors (for details see text). No error indicates that this parameter was fixed in the fit

Remarks	χ^2/ν	T_{kin} (MeV)	η_f	$\langle\beta_T\rangle$	T_{chem} (MeV)	μ_B (MeV)	Δ
			PHENIX data				
narrow profile (A)	101/57	143.0 ± 6.8	0.745 ± 0.031	0.450 ± 0.016	173.3 ± 2.0	35.9 ± 4.2	50
wide profile (A$'$)	98/57	142.2 ± 7.3	0.558 ± 0.022	0.414 ± 0.014	173.0 ± 2.0	37.1 ± 4.3	5
low m_T - narrow	80/39	137.0 ± 7.4	0.759 ± 0.033	0.457 ± 0.017	172.5 ± 2.0	35.0 ± 4.3	50
low m_T - wide	72/39	128.5 ± 8.3	0.609 ± 0.026	0.444 ± 0.015	172.5 ± 2.1	35.8 ± 4.4	5
no weak decays - narrow	116/57	144.7 ± 7.5	0.730 ± 0.033	0.442 ± 0.016	186.4 ± 2.5	38.6 ± 4.6	50
no weak decays - wide	109/57	141.3 ± 8.0	0.557 ± 0.024	0.413 ± 0.015	185.5 ± 2.6	39.9 ± 4.6	5
$T_{kin} = T_{chem}$ - narrow	163/59	165	0.633 ± 0.009	0.392 ± 0.004	165	43.0 ± 5.1	50
$T_{kin} = T_{chem}$ - wide	158/59	165	0.482 ± 0.006	0.366 ± 0.004	165	43.8 ± 5.1	5
STAR T - narrow	186/58	94.8	0.962 ± 0.007	0.548 ± 0.003	163.6 ± 1.5	35.1 ± 4.1	50
STAR T - wide	206/58	83.6	0.730 ± 0.005	0.509 ± 0.002	161.4 ± 1.5	37.5 ± 4.1	5
			STAR data				
narrow profile (B)	19/36	94.8 ± 7.9	1.037 ± 0.031	0.578 ± 0.012	165.3 ± 2.2	31.2 ± 2.5	50
wide profile (B$'$)	36/36	83.6 ± 8.3	0.984 ± 0.033	0.622 ± 0.013	174.4 ± 2.9	33.8 ± 2.7	5
no weak decays - narrow	22/36	88.0 ± 7.1	1.038 ± 0.030	0.578 ± 0.012	174.6 ± 2.6	33.0 ± 2.7	50
no weak decays - wide	41/36	77.7 ± 7.4	0.984 ± 0.032	0.622 ± 0.013	184.9 ± 3.3	36.0 ± 2.8	5
$T_{kin} = T_{chem}$ - narrow	55/38	165	0.920 ± 0.020	0.530 ± 0.008	165	32.4 ± 2.5	50
$T_{kin} = T_{chem}$ - wide	75/38	165	0.781 ± 0.019	0.535 ± 0.009	165	34.0 ± 2.5	5
PHENIX T - narrow	41/37	143.0	0.944 ± 0.029	0.540 ± 0.012	164.4 ± 2.4	32.1 ± 2.5	50
PHENIX T - wide	61/37	142.2	0.858 ± 0.032	0.570 ± 0.014	170.4 ± 3.2	34.2 ± 2.6	5
			PHENIX + STAR data				
narrow profile (C)	206/98	112.3 ± 3.3	0.886 ± 0.014	0.515 ± 0.006	165.0 ± 1.0	34.5 ± 2.2	50
wide profile	323/98	108.3 ± 4.0	0.673 ± 0.012	0.479 ± 0.006	160.9 ± 1.0	38.1 ± 2.1	5
no weak decays - narrow	230/98	109.4 ± 3.5	0.888 ± 0.015	0.516 ± 0.006	175.5 ± 1.3	36.7 ± 2.3	50
no weak decays - wide	332/98	103.8 ± 4.2	0.680 ± 0.012	0.483 ± 0.006	170.4 ± 1.2	40.3 ± 2.3	5
$T_{kin} = T_{chem}$ - narrow	389/100	165	0.672 ± 0.006	0.413 ± 0.003	165	38.5 ± 2.1	50
$T_{kin} = T_{chem}$ - wide	470/100	165	0.517 ± 0.004	0.388 ± 0.002	165	40.1 ± 2.1	5

clude resonances [30]. These yield similar average flow ($\langle\beta_T\rangle = 0.47 \pm 0.01$) velocities but smaller kinetic freeze-out temperatures ($T_{kin} = 121 \pm 4\,\text{MeV}$) – this difference is consistent with the influence of resonance decays.

Fits assuming a unique temperature of $T = 165\,\text{MeV}$ for both kinetic and chemical freeze-out as in [31] are again much worse in fit quality for both shapes of the source distribution, as can be seen from the large χ^2 in Table 2. The assumption of simultaneous kinetic and chemical freeze-out underlying this fit is questionable, but I will still consider such a fit once more below. One might argue that the transverse mass range used in these fits does include possible contributions of hard scattering. However, fits which use data only for low m_T ($m_T - m_0 < 1.5\,\text{GeV}/c$) yield very similar results as seen in Table 2.

Finally, a simultaneous fit to STAR and PHENIX data has been performed, where the STAR data have been rescaled by a factor 0.92 (ratio of the number of participants) to account for the different centrality selection.

Please note that such a simultaneous fit is only successful if one includes the systematic errors. Considering just statistical errors, the data from the two experiments could not be consistently described by this model. The results are also given in Table 2, the best fit (C) is compared to the data in Fig. 10. Fit (C) is obtained using $\Delta = 50$ and describes the data reasonably well with $\chi^2/\nu = 206/98$. Chemical parameters change relatively little. As might be expected the kinetic parameters are intermediate between those for the individual experiments, one finds $T_{kin} = 112.3\,\text{MeV}$ and $\langle\beta_T\rangle = 0.515$. Once again a fit using $T_{kin} = T_{chem} = 165\,\text{MeV}$ is significantly worse.

5 Discussion

The results for SPS and RHIC data may now be compared to each other. In both cases a box-like profile is favored over a Gaussian-like profile. It was already discussed in [7]
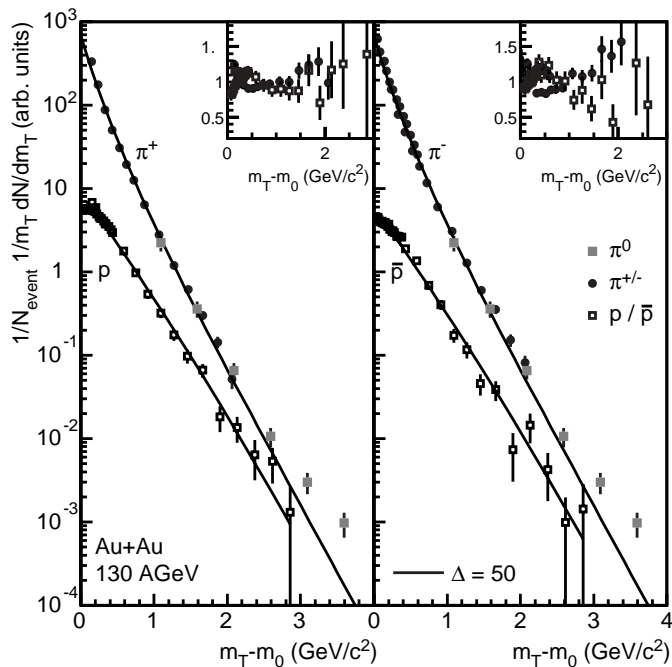
Fig. 10. Transverse mass distributions of pions and (anti)protons for central Au+Au collisions at $\sqrt{s_{NN}} = 130\,\mathrm{GeV}$ from the PHENIX and STAR experiments. The lines show a simultaneous fit (C) from Table 2. The inset shows the ratio of the data to the fit

that a box-like profile would be required in case of a large flow velocity, and this was also found to be the preferred profile in [8]. Such a distribution with little or no "tail" to higher velocities is also closer to expectations from true hydrodynamic calculations [28]. In both cases (SPS and RHIC) there are fits with a range of flow velocities, depending mainly on the experiment that one concentrates on. At the SPS the range of velocities is $\langle \beta_T \rangle = 0.48 - 0.55$ and the analysis presented here does not allow to constrain this value further. At RHIC a combined fit is possible, which yields as the most likely value $\langle \beta_T \rangle = 0.515$. Similarly the range of kinetic freeze-out temperatures for the SPS is $T_{kin} = 76 - 122\,\mathrm{MeV}$, while the RHIC value appears to be $T_{kin} = 112.3\,\mathrm{MeV}$. Apparently this analysis indicates that the flow velocities at SPS and RHIC may be similar, and there is no clear indication of stronger collective flow at RHIC as found in [32]. It can, however, be seen in [32] that this is strongly influenced by the proton and antiproton spectra from STAR used in the analysis, which show a much larger inverse slope than the PHENIX results.

Both for SPS and RHIC there are still considerable uncertainties which are related to the experimental data themselves. For the SPS these imply large uncertainties for the extrapolation of the hydrodynamical fits to higher m_T. Still, if we attempt to ascribe particle production at low m_T in heavy-ion collisions at the SPS to hydrodynamic scenarios, the extrapolation of the hydrodynamic contribution to high m_T will yield a considerable contribution of hydrodynamic production.

For RHIC the measurement of protons and antiprotons at higher m_T does provide additional constraints and excludes some of the extreme scenarios. A simultaneous fit to STAR and PHENIX has been performed, which yields a reasonable agreement with the available data. In the following I will assume that this fit describes the contribution of a hydrodynamic source to particle emission. It does describe the spectra almost entirely at low m_T. At higher m_T the fit starts to deviate, which is not surprising, as one would expect additional production mechanisms, especially hard scattering, to play a role there. However, this hydrodynamic contribution may be still significant even at high momenta – this would be of particular relevance to any study of hard scattering, because to be able to obtain information on hard scattering production one would have to know this hydrodynamic contribution and take it into account.

A simple partitioning of the produced particles into either hydrodynamic or hard scattering production is not possible. If one believes that equilibration is taking place in these collisions, there will almost necessarily be parts of the reaction volume that are only partially equilibrated. At RHIC the high p_T part of the non-equilibrated spectrum (with a power-law shape from hard scattering) should have a larger inverse slope than the equilibrated spectrum (similar to exponential). So in this case equilibration through multiple collisions will slow particles down and soften the spectrum. As the degree of equilibration will vary throughout the reaction volume, the spectrum might be a superposition of a range of spectra between the one from the initial collisions and a thermalized one.

At this point one does not necessarily need to distinguish between parton and hadron degrees of freedom. Thus, parton energy loss would just be one possible equilibration mechanism. While it is not possible to precisely predict how close the final distribution would be to a thermal (hydrodynamic) distribution, the latter can be taken as a limiting case. If hard scattered partons are completely quenched, one will still end up with a thermal distribution as a minimum yield. Any excess over this minimum might be due to non-equilibrated contributions, either true hard scattering production or not completely equilibrated production, which still has a higher average momentum than the thermal.

The discussion in this paper assumes that the spectra in the intermediate momentum region can be described by thermal distributions. This is not completely correct, as e.g. even hard scatterings will produce some lower momentum component. However, as any comparison of pure hydrodynamics to data, I will assume for the following that this non-thermal contribution at low and intermediate p_T is negligible.

In Fig. 11 ratios of the simultaneous fit (C) to the experimental data, i.e. the fractions R_{hydro} of the produced particles accounted for by the hydrodynamic parameterization, are shown for neutral pions (solid squares) and for protons+antiprotons (open circles) as a function of p_T.
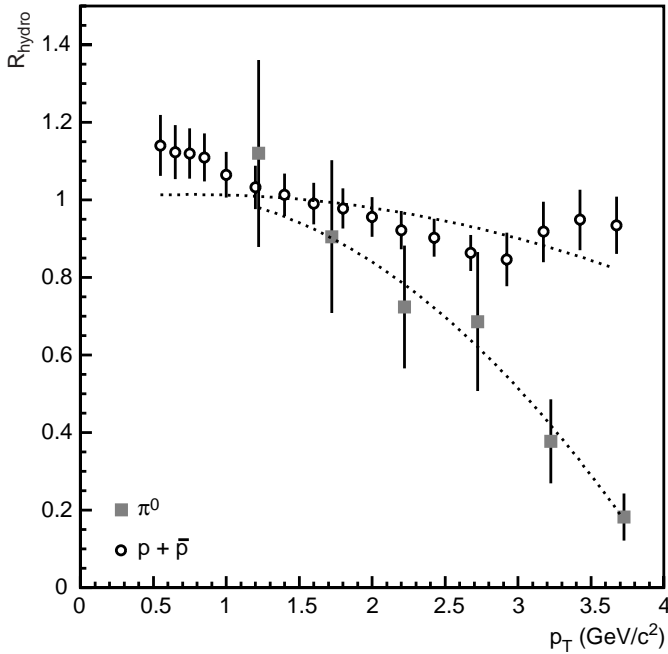
Fig. 11. Fraction of the hydrodynamic component of the neutral pion and proton+antiproton yield using fit C from Table 2. The dotted line shows a fit of a Woods-Saxon function to the data (see text)

The proton+antiproton yield is reasonably described by this fit in the entire p_T range investigated, as can be seen by the more or less constant ratio. The hydrodynamic contribution to pions depends more strongly on p_T. While here hydrodynamics dominates also at lower p_T, there is a steady decrease of the contribution towards higher p_T. Still even for $p_T \geq 3\,\mathrm{GeV}/c$ the hydrodynamic contribution to the pion yield is close to 40%.

The not completely thermalized part of the emitted hadrons will reflect itself in other observables. A p_T dependent non-thermalized contribution to the spectrum will be related to a p_T dependent deviation of the measured elliptic flow v_2 from the purely hydrodynamic behavior, because the latter relies on equilibration achieved earlier in the collision history than kinetic freeze-out. Quantitative estimates of this are difficult, as the partially thermalized contribution will lead to an unknown contribution to v_2. Full hydrodynamic calculations, when applied to elliptic flow and particle spectra, should be able to extract more information on this.

6 Summary

Results of hydrodynamic fits to momentum spectra at mid-rapidity in heavy ion reactions at the SPS and at RHIC have been presented. While at RHIC a simultaneous description of STAR and PHENIX data is possible, when systematic errors are taken into account, there are still unresolved differences at SPS depending on the experiment used. At SPS a chemical temperature of $T_{chem} \approx 145\,\mathrm{MeV}$ and a baryo-chemical potential of $\mu_B \approx 190\,\mathrm{MeV}$

have been obtained. This chemical temperature is slightly smaller than values obtained from rapidity integrated yields. At RHIC the corresponding values are $T_{chem} \approx 165\,\mathrm{MeV}$ and $\mu_B \approx 35\,\mathrm{MeV}$. The kinetic parameters are $T_{kin} = 76 - 122\,\mathrm{MeV}$ and $\langle \beta_T \rangle = 0.48 - 0.55$ at SPS and $T_{kin} \approx 110\,\mathrm{MeV}$ and $\langle \beta_T \rangle \approx 0.52$ at RHIC when using a velocity profile similar to a box profile. The momentum spectra at RHIC are broader than at the SPS. However, this analysis does not prove a significantly stronger transverse flow at RHIC, the change in the momentum spectra might also be due to a higher freeze-out temperature. At high transverse momenta the spectra of protons can be nicely described at RHIC. The pion spectra leave room for additional particle production mechanisms (e.g. hard scattering) at high p_T. Estimates of the suppression of hard scattering should, however, take the non-negligible contribution from a hydrodynamic source into account. Important hydrodynamic contributions in spectra at high p_T require even stronger quenching of hard scattering production. In return, quenching is a necessary condition to achieve locally equilibrated distributions.

References

1. E. Schnedermann, J. Sollfrank, U. Heinz, Phys. Rev. C **48**, 2462 (1993)
2. S. Chapman, J.R. Nix, U. Heinz, Phys. Rev. C **52**, 2694 (1995)
3. P. Braun-Munzinger et al., Phys. Lett. B **344**, 43 (1995)
4. U.A. Wiedemann, U. Heinz, Phys. Rev. C **56**, 3265 (1997)
5. NA49 Collaboration, H. Appelshäuser et al., Eur. Phys. J. C **2**, 661–670 (1998)
6. WA80 Collaboration, R. Albrecht et al., Eur. Phys. J. C **5**, 255 (1998)
7. WA98 Collaboration, M.M. Aggarwal et al., Phys. Rev. Lett **83**, 926 (1999)
8. B. Tomasik, U.A. Wiedemann, U. Heinz, preprint nucl-th/9907096
9. PHENIX Collaboration, K. Adcox et al., Phys. Rev. Lett. **88**, 022301 (2002)
10. STAR Collaboration, C. Adler et al., Phys. Rev. Lett. **87**, 182301 (2001)
11. PHENIX Collaboration, K. Adcox et al., submitted to Phys. Rev. Lett., preprint nucl-ex/0204005
12. NA49 Collaboration, P.G. Jones et al., Nucl. Phys. A **610**, 188c (1996)
13. NA44 Collaboration, I.G. Bearden et al., submitted to Phys. Rev. C, preprint nucl-ex/0205002
14. NA49 Collaboration, S.V. Afanasiev et al., submitted to Phys. Rev. C, preprint nucl-ex/0202019
15. NA49 Collaboration, S.V. Afanasiev et al., proceedings of Quark Matter 2002, Nantes, France

16. P. Braun-Munzinger, I. Heppe, J. Stachel, Phys.Lett. B **465**, 15–20 (1999)
17. M. Gazdzicki, private communication
18. WA98 Collaboration, M.M. Aggarwal et al., Eur. Phys. J. **C 23**, 225–236 (2002)
19. J. Sollfrank, U. Heinz, H. Sorge, N. Xu, Phys. Rev. C **59**, 1637 (1999)
20. M. Kaneta, N. Xu, J. Phys. G **27**, 589 (2001)
21. F. Becattini, J. Cleymans, A. Keränen, E. Suhonen, K. Redlich, Phys. Rev. C **64**, 024901 (2001)
22. PHENIX Collaboration, K. Adcox et al., Phys. Rev. Lett. **88**, 242301 (2002)
23. PHENIX Collaboration, J. Velkovska et al., talk at ICPA-QGP 2001 Jaipur, to be published in Pramana - Journal of Physics
24. STAR Collaboration, C. Adler et al., Phys. Rev. Lett. **87**, 262302 (2001)
25. STAR Collaboration, K. Schweda et al., proceedings of RIKEN BNL Workshop Vol.42 (2002) p.57,eds. M. Gyulassy, D. Kharzeev, N. Xu, Brookhaven National Laboratory, Upton, NY 11973-500, USA
26. M. Calderon, PhD thesis, Yale university, 2001, preprint nucl-ex/0111004
27. PHENIX Collaboration, K. Adcox et al., in preparation
28. P. Huovinen, P.F. Kolb, U. Heinz, P.V. Ruuskanen, S.A. Voloshin, Phys. Lett. B **503**, 58–64 (2001)
29. P. Braun-Munzinger, D. Magestro, K. Redlich, J. Stachel, Phys. Lett. B **518**, 41–46 (2001)
30. PHENIX collaboration, J.M. Burward-Hoy et al., talk at Quark Matter 2002, Nantes, to be published in Nucl. Phys. A, preprint nucl-ex/0210001
31. W. Broniowski, W. Florkowski, Phys.Rev.Lett. **87**, 272302 (2001)
32. N. Xu, M. Kaneta, Nucl. Phys. **A 698**, 306c (2002)